JCI insight

RESEARCH ARTICLE

# Irradiation abolishes smooth muscle investment into vascular lesions in specific vascular beds

**Alexandra A.C. Newman,[1,2] Richard A. Baylis,[1,2] Daniel L. Hess,[1,2] Steven D. Griffith,[1,2] Laura S. Shankman,[1,3] Olga A. Cherepanova,[1,3] and Gary K. Owens[1,3]**

[1]Robert M. Berne Cardiovascular Research Center, [2]Department of Biochemistry and Molecular Genetics, and [3]Department of Molecular Physiology and Biological Physics, University of Virginia, Charlottesville, Virginia, USA.

**The long-term adverse effects of radiotherapy on cardiovascular disease are well documented. However, the underlying mechanisms responsible for this increased risk are poorly understood. Previous studies using rigorous smooth muscle cell (SMC) lineage tracing have shown abundant SMC investment into atherosclerotic lesions, where SMCs contribute to the formation of a protective fibrous cap. Studies herein tested whether radiation impairs protective adaptive SMC responses during vascular disease. To do this, we exposed SMC lineage tracing (*Myh11*-ER$^{T2}$Cre YFP$^{+}$) mice to lethal radiation (1,200 cGy) followed by bone marrow transplantation prior to atherosclerosis development or vessel injury. Surprisingly, following irradiation, we observed a complete loss of SMC investment in 100% of brachiocephalic artery (BCA), carotid artery, and aortic arch lesions. Importantly, this was associated with a decrease in multiple indices of atherosclerotic lesion stability within the BCA. Interestingly, we observed anatomic heterogeneity, as SMCs accumulated normally into lesions of the aortic root and abdominal aorta, suggesting that SMC sensitivity to lethal irradiation occurs in blood vessels of neural crest origin. Taken together, these results reveal an undefined and unintended variable in previous studies using lethal irradiation and may help explain why patients exposed to radiation have increased risk for cardiovascular disease.**

## Introduction

Since its introduction in 1951, radiation exposure followed by bone marrow transplantation (BMT) has become a key technique for both medical practice and biomedical research (1). Indeed, this procedure has been used in over 100,000 basic science papers, and stem cell transplantation has been used to treat over a million patients (2). Although it has greatly improved the survival rates for multiple malignancies, exposure to levels of radiation necessary to deplete the bone marrow have long-term side effects, including a profound increase in cardiovascular disease (CVD). Indeed, pediatric cancer patients, who are often treated with radiotherapy or BMT, are 7 times more likely to die from a cardiovascular complication, making CVD the leading cause of nonmalignant death in these patients (3). Further, women treated with radiotherapy for breast cancer have a dose-dependent increase in CVD risk, which was shown to be independent of traditional risk factors (4). This has motivated extensive research on the cardiovascular effects of radiation in mouse models of atherosclerosis. Consistent with the clinical data, multiple studies have shown that lethal irradiation results in decreased indices of atherosclerotic lesion stability, including reduced collagen content, increased macrophage marker staining, and increased intraplaque hemorrhage (5–7). However, there is a high level of unexplained variability in the literature as to the effect of radiation exposure on different vascular beds. For example, lesion size has been shown to increase in the aortic sinus yet decrease in the aortic arch (6). Although there are many possible causes for this heterogeneity, we hypothesize that it is due in part to differences in the sensitivity of smooth muscle cells (SMCs) to radiation in different vascular beds.

A critical role for SMCs in atherosclerosis has become increasingly clear, due in large part to the development of rigorous SMC lineage tracing and simultaneous conditional gene knockout studies in long-term Western diet–fed (WD-fed) *Apoe*$^{-/-}$ mice (8–10). Briefly, studies have shown that lesion SMCs are derived from a subset of mature Myh11$^{+}$ medial SMCs that clonally expand to populate the lesion (11–13). Further, >80% of the SMCs within atherosclerotic lesions lack expression of characteristic SMC markers, and,

**Authorship note:** AACN and RAB contributed equally to this work.

**Conflict of interest:** The authors have declared that no conflict of interest exists.

**Submitted:** March 12, 2018
**Accepted:** June 29, 2018
**Published:** August 9, 2018

**Reference information:**
*JCI Insight*. 2018;3(15):e121017.
https://doi.org/10.1172/jci.insight.121017.

of these, nearly 50% have activated markers of macrophages, mesenchymal stem cells, or myofibroblasts and, thus, would have been missed or misidentified in previous studies (9). Moreover, SMC-specific knockout studies have shown that SMCs can have key beneficial or detrimental effects on lesion pathogenesis, depending on the nature of their phenotypic transitions (8–10, 14). For example, Klf4-dependent transitions, including formation of SMC-derived macrophage marker$^+$ foam cells (9) exacerbated lesion pathogenesis, while Oct4-dependent transitions (10) were protective, including being critical for investment of SMCs into the fibrous cap. The studies herein examine the effects of lethal irradiation on the contribution of SMCs to atherosclerosis lesion pathology and surgically induced neointima formation.

## Results

To determine the effect of lethal gamma radiation on SMC during atherosclerosis, we injected SMC lineage tracing *Myh11*-ER$^{T2}$Cre ROSA-STOP-eYFP *Apoe*$^{-/-}$ (SMC-YFP, *Apoe*$^{-/-}$) mice with tamoxifen from 6–8 weeks of age (Figure 1A). Mice were then exposed to whole-body lethal radiation (1,200 cGy) using a cesium-137 irradiator, with subsequent BMT at 9 weeks of age, followed by 6 weeks of rest to allow for bone marrow engraftment. Nonirradiated non-BMT littermates were used as controls. We placed mice on WD for 18 weeks to induce atherogenesis (Figure 1B). Flow cytometric analyses of blood at the time of harvest showed >95% bone marrow engraftment (Supplemental Figure 1; supplemental material available online with this article; https://doi.org/10.1172/jci.insight.121017DS1). Vessels were harvested and analyzed for indices of lesion stability and cellular composition. Of major significance, we found that SMCs failed to accumulate in any of the brachiocephalic artery (BCA) lesions (Figure 1E) from lethally irradiated mice, as assessed by YFP staining at multiple locations along the length of the BCA (Figure 2, B and C). In contrast, in the control mice, >85% of the BCA lesions had YFP$^+$ SMC accumulation, consistent with the hundreds of SMC-YFP, *Apoe*$^{-/-}$ mice previously analyzed in our lab and others (Figure 2, A and C) (8–10, 12, 14). Furthermore, to assess the functional consequences of SMC loss in the BCA, we found that BCA lesions from irradiated mice exhibited decreases in multiple indices of lesion stability, including significant increases in intraplaque hemorrhage ($P$ = 0.0003) and necrotic core area ($P$ = 0.0082) and a significant reduction in collagen content ($P$ = 0.0186, Figure 2, D–F). However, despite reductions in multiple indices of lesion stability, we found that vessel morphology, including external elastic lamina and lesion area, was not significantly changed (Figure 2, G and H). Importantly, these observations were consistent despite using multiple bone marrow donor lines including from CD45.1, tdTomato, or dsRed mice (see Methods, Figure 1B). Taken together, radiation induces loss of SMC accumulation and results in detrimental effects on multiple indices of lesion stability within BCA lesions, highlighting an unexpected and highly significant side effect of lethal irradiation.

To determine if other vascular beds exhibited a similar loss of SMC accumulation, we examined multiple vascular locations, including the aortic arch, aortic root (Figure 1E), and abdominal, renal, and iliac arteries. Similar to our observations in the BCA, lesions in the aortic arch of all irradiated animals lacked SMC accumulation (Figure 3, A, B, and G). However, all other vascular beds showed similar SMC accumulation in both the irradiated and control mice, including in the aortic root (Figure 3, C, D, and H) and the abdominal aorta (Figure 3, E, F, and I) and renal and iliac arteries, suggesting that the SMCs of aortic arch and BCA are uniquely sensitive to radiation. Of interest, SMCs from these two sites, unlike any of the other vascular sites tested, are derived from the neural crest (NC) (15).

To determine if ionizing radiation has a direct effect on the vascular SMCs that could explain their absence in BCA lesions, we harvested vessels from mice at 1, 4, and 7 days after irradiation and BMT and from age-matched nonirradiated controls (Figure 1C). Of major interest, lethal irradiation resulted in significantly increased YFP$^+$TUNEL$^+$ cells in the BCA vessel media at 1 and 4 days after irradiation, which decreased to the level of controls by 7 days (Figure 4, A and B). Surprisingly, increased YFP$^+$TUNEL$^+$ staining was not observed in the aortic root or coronary or pulmonary vessels (Figure 4, C–E), suggesting that the medial Myh11$^+$ SMCs from various vascular beds have different susceptibilities to radiation-induced DNA double-strand breaks. In the BCA media, the increased YFP$^+$TUNEL$^+$ staining was not associated with a decrease in the number of YFP$^+$ cells (Figure 4F). To determine if the double-strand DNA breaks were associated with increased SMC apoptosis, we assessed the percentage of YFP$^+$ cleaved caspase-3$^+$ cells in the BCA and found >1% apoptotic SMCs at day 1 and 4 (Figure 4G), suggesting that the vast majority of TUNEL$^+$ SMCs did not undergo subsequent apoptosis. At the time of radiation exposure, we injected mice with a single pulse of BrdU to assess SMC proliferation directly after radiation. Consistent with the literature, we

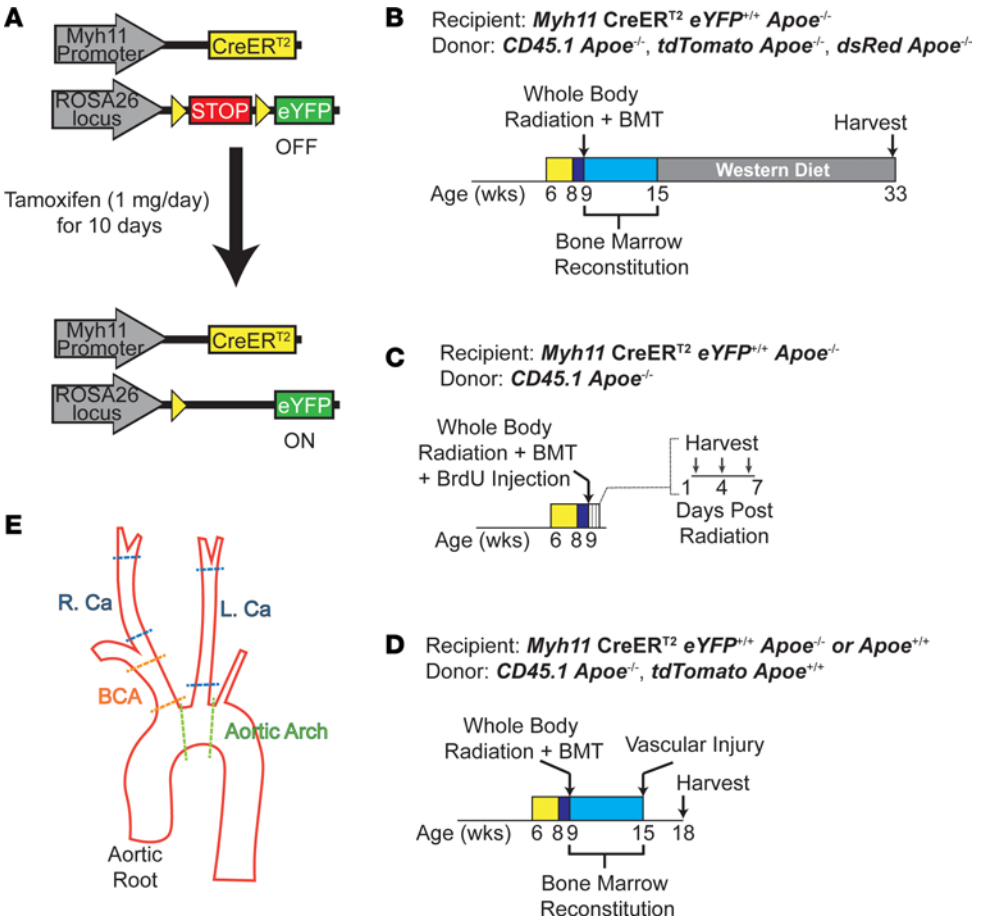


**Figure 1. Experimental design.** (**A**) Schematic of *Myh11*-CreER$^{T2}$, ROSA*26* STOP-flox eYFP$^{+/+}$ (SMC-YFP) mice. Upon tamoxifen injection, any cell transcribing *Myh11* underwent excision of a floxed STOP codon in front of an eYFP transgene driven by the ROSA26 locus, allowing for permanent eYFP labeling of SMCs and their progeny. (**B–D**) SMC-YFP, *Apoe*$^{-/-}$ littermates at 9 weeks of age were subjected to 0 (nonirradiated, non-BMT controls) or 1,200 cGy of ionizing radiation and then administered >1 × 10$^6$ bone marrow cells (BMT). (**B**) Following 6 weeks of recovery to allow bone marrow engraftment, the mice were placed on a Western diet for 18 weeks to induce atherosclerosis formation. (**C**) Directly after radiation, mice were given a single BrdU pulse (10 mg/ml) and harvested at 1, 4, or 7 days after irradiation or 5 days after BrdU pulse for nonirradiated, non-BMT controls. (**D**) Following 6 weeks of recovery to allow bone marrow engraftment, mice underwent carotid ligation or femoral wire injury for 21 days. Bone marrow donor lines are indicated for each experiment. (**E**) Delineation of cut sites for vessels excised from the aortic outflow tract

found that very few medial SMCs proliferate in the absence of vascular injury, and, even after irradiation, the maximum percentage of proliferating YFP$^+$ cells was <2% (Figure 4H), which was confirmed by Ki67 staining. Thus, SMCs within the BCA appear to be uniquely susceptible to γ radiation, as demonstrated by increased TUNEL staining, which suggests that part of the effect of lethal irradiation-induced loss of SMC accumulation in lesions is intrinsic to SMCs in this vascular bed.

To determine if the loss of YFP$^+$ SMC accumulation was unique to atherosclerosis, we performed carotid ligation and femoral injury, two models of surgically induced vascular injury, on *Myh11*-ER$^{T2}$Cre, ROSA26 STOP-flox eYFP$^{+/+}$ mice with and without *Apoe* knockout (SMC-YFP) following irradiation and BMT. Consistent with results in the BCA and aortic arch, we observed a profound reduction in SMC investment into neointimal lesions resulting from carotid ligation (Figure 1, D and E, and Figure 5). Indeed, none of the irradiated mice demonstrated SMC investment into the neointima (Figure 5, B and C), whereas 90% of the control mice had significant YFP$^+$ SMC investment (Figure 5, A and C). However, SMC accumulation in the neointima induced by femoral injury showed SMC accumulation, regardless of radiation exposure. These data are consistent with our results in atherosclerosis, indicating that radiation has different effects on SMC accumulation in different vascular beds. Moreover, these additional models indicate that the observed results were not a function of the mouse age, diet, type of vascular insult, BMT donor, or hyperlipidemia.

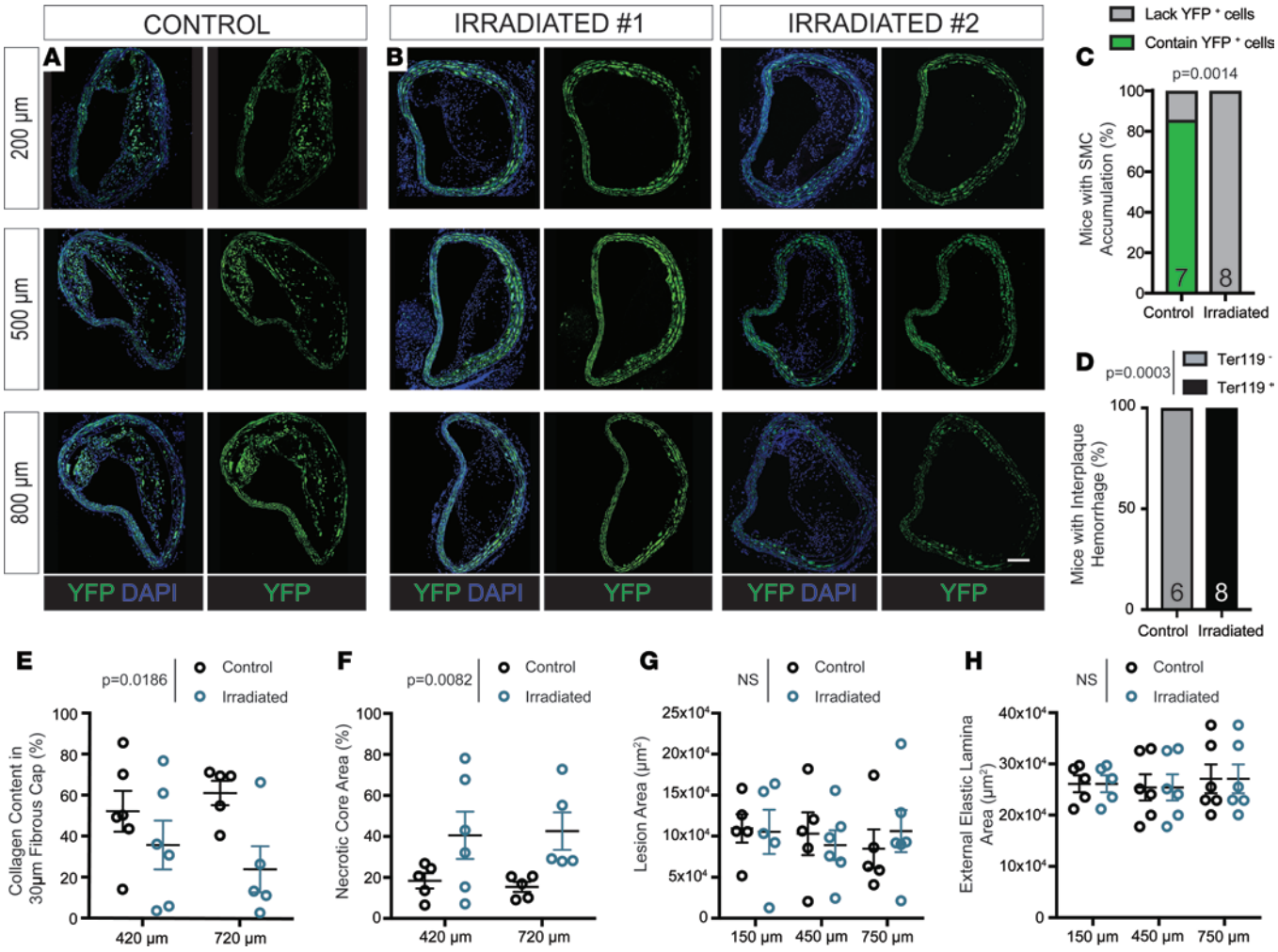


**Figure 2. SMCs fail to invest within brachiocephalic atherosclerotic lesions following lethal irradiation and BMT; these changes are associated with decreased indices of lesion stability.** SMC-YFP, *Apoe*$^{-/-}$ mice received 1,200-cGy whole-body radiation and BMT followed by 18 weeks of WD to induce atherosclerosis lesion development. (**A**) High-resolution confocal imaging shows consistent YFP$^+$ cell accumulation in brachiocephalic (BCA) lesions of control mice. (**B**) Lethally irradiated animals show loss of YFP$^+$ cell accumulation in BCA lesions at 3 locations past the aortic arch. (**C**) Fisher's exact test quantifying the percentage of control and irradiated animals that demonstrate YFP$^+$ cell accumulation in BCA lesions. (**D**) Fisher's exact test quantifying the percentage of animals with intraplaque hemorrhage in at least 1 of 3 locations along the BCA. (**E**) The percentage of collagen pixels in the 30-µm lesion cap area was significantly decreased after lethal irradiation. (**F**) The necrotic core area was significantly increased in BCA lesions after lethal irradiation. (**G** and **H**) Lesion area (**G**) and external elastic lamina area (**H**) were not changed between control and radiated animals **E**–**H**. Data were assessed by 2-way ANOVA. Data represent mean ± SEM. Sample number is indicated in the graph. Scale bar: 100 µm.

## Discussion

Taken together, the present study reveals that an unintended and highly unexpected consequence of lethal irradiation is a profound impairment of SMC accumulation in vascular lesions that form in the BCA, aortic arch, and carotid artery. It is interesting to speculate based on the vascular patterning of these effects that they are due to differences in the embryologic origin of the SMCs. Indeed, fate-mapping studies have revealed that SMCs develop from at least 8 unique embryologic origins and that this appears to affect the behavior of the mature SMCs (15). For example, TGF-β stimulation of NC-derived cultured SMCs results in increased DNA synthesis, while mesoderm-derived SMCs show the opposite response (16–18). Loss of SMC accumulation in vascular lesions is highly consistent with vessels where SMCs are derived from the NC. This is perhaps best illustrated by the profound effect of whole-body γ radiation in the aortic arch but lack of effect in the adjacent aortic root.

Although studies provide compelling evidence that investment of NC-derived SMCs within lesions is lost following lethal irradiation, results do not distinguish if this is driven by direct intrinsic effects of radiation on SMCs themselves or through secondary effects on other cell types, tissues, or the lesion microenvironment.

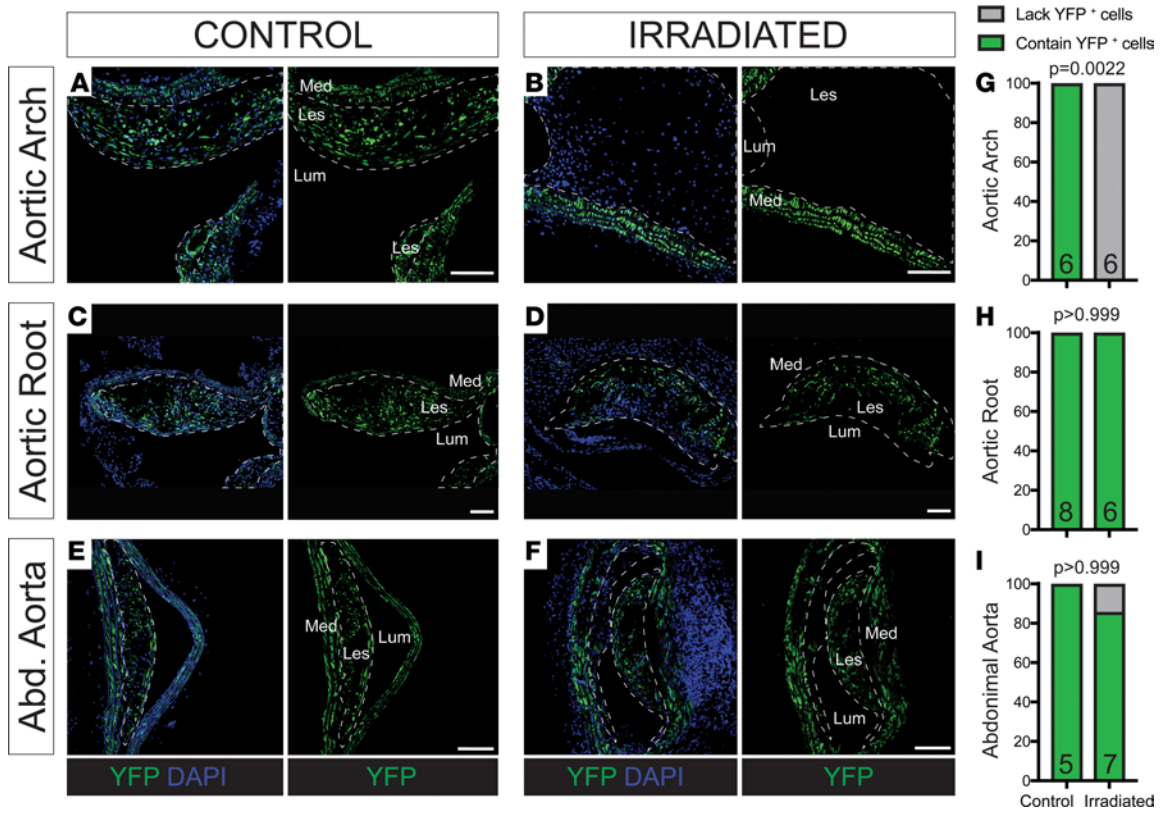


**Figure 3. Vascular SMCs show heterogeneous investment in atherosclerotic lesions depending on vascular bed.** (**A** and **B**) YFP$^+$ cell accumulation was not observed in irradiated lesions but was observed in controls within the aortic arch. (**C** and **D**) Lesions within the aortic root and (**E** and **F**) abdominal aorta consistently had YFP$^+$ cell accumulation in both control and irradiated mice. (**G–I**) Fisher's exact test quantifying the percentage of control and irradiated animals with lesions that demonstrate YFP$^+$ cell accumulation at each location. Sample number is indicated in the graph. Scale bar: 100 μm.

The fact that we only observed this phenotype in NC-derived vascular beds, despite using whole-body radiation, suggests that the local environment plays a critical role. However, the underlying mechanisms are likely to be highly complex. For example, radiation-induced damage to local endothelial cells could inhibit the expression of factors required to stimulate SMC investment or induce secretion of factors that inhibit investment into lesions (19). It is also possible that functional changes in the engrafted hematopoietic stem cells that seed the bone marrow niche following BMT selectively affect SMCs or that radiation may affect one or more of the other NC-derived cell populations shown to play a critical role in the remodeling of the branchial arch vessels during vascular development (20).

Our observations of increased YFP$^+$TUNEL$^+$ cells selectively in the BCA suggest that radiation is directly and/or selectively affecting the Myh11$^+$ medial SMC population and preventing SMCs from accumulating within lesions. However, further study is required to determine if there are other contributing factors from circulating cells or the local environment. If radiation was directly targeting the NC-derived SMCs, this would appear to be inconsistent with the widely accepted dogma that radiation primarily affects highly proliferative and poorly differentiated cells (21). Indeed, SMCs are known to have a very low proliferation rate within mature blood vessels (~0.1%) (22, 23) and are therefore considered one of the most radioresistant cell types. However, several recent studies (12, 13), using multicolor SMC clonal analysis, have shown that SMCs in BCA and carotid lesions are derived from oligoclonal expansion of a small number of medial SMCs. Thus, it is possible that a subpopulation of medial Myh11$^+$ SMCs in NC-derived vascular beds are poised to undergo clonal expansion, and perhaps these cells are susceptible to radiotherapy. Interestingly, SMCs located at the tip of muscularized pulmonary arterioles, which are also NC derived (24), have been shown to be primed to clonally expand following hypoxia-induced pulmonary hypertension (25). Perhaps there is a similar subpopulation among the aortic SMCs. Consistent with this idea, a recent study (26) has shown that a subset of differentiated SMCs (using *Myh11*-ER$^{T2}$Cre) express the mouse stem cell marker Sca1. It is interesting to speculate

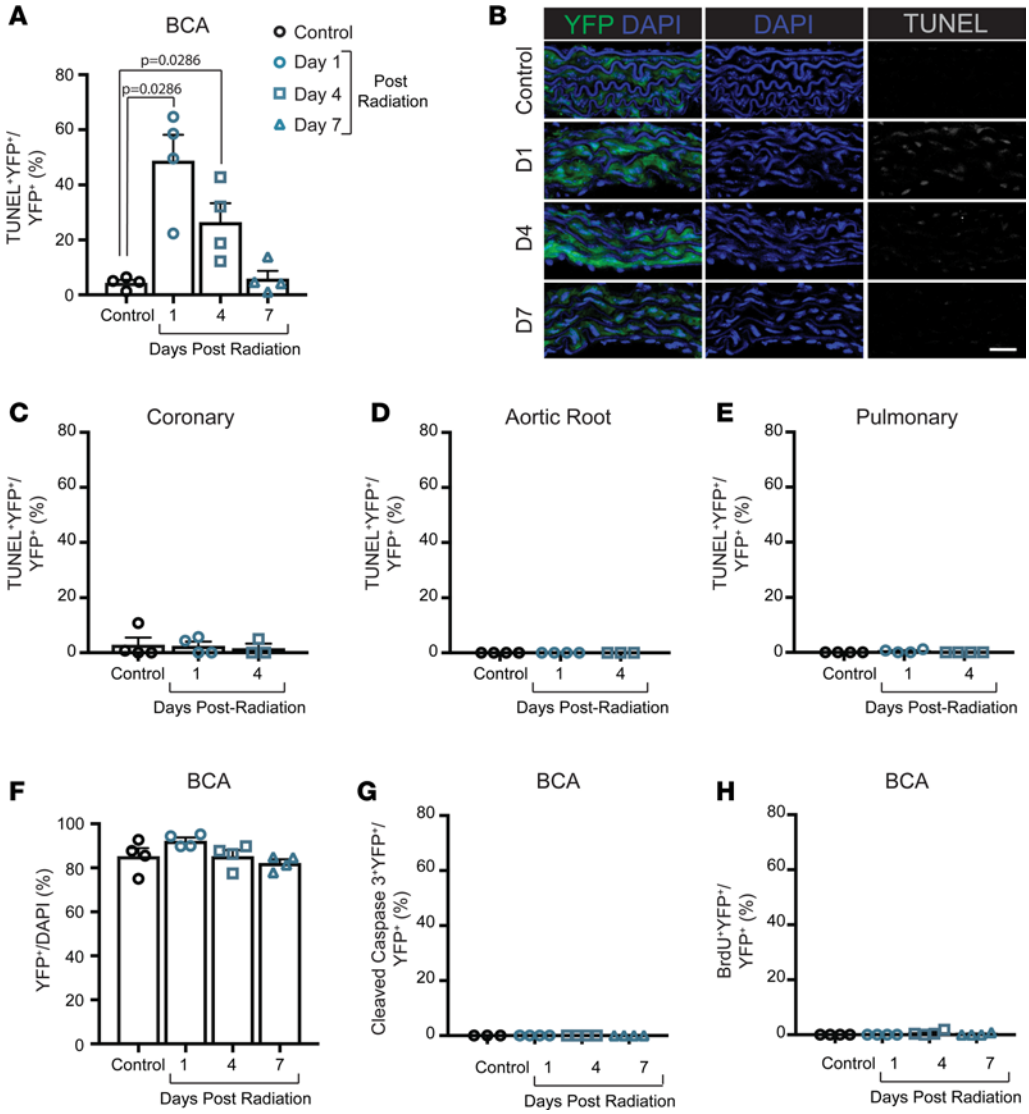


**Figure 4. Radiation induces DNA damage only in BCA SMCs but does not result in increased apoptosis or proliferation.** (**A** and **B**) Lethal radiation exposure results in significantly more TUNEL$^+$YFP$^+$ cells within the brachiocephalic artery (BCA) at day 1 and 4 after radiation. (**C–E**) SMCs do not show increased TUNEL$^+$ cells in the media of the coronary (**C**), aortic root (**D**), or pulmonary vessels (**E**). (**F**) There was no difference in the number of YFP$^+$ cells in the media of the BCA. (**G**) There was no difference in the number of cleaved caspase-3$^+$YFP$^+$ cells in the media of the BCA. (**H**) Nor was there any change in the number of cells incorporating BrdU following lethal radiation exposure. Data were assessed by Mann Whitney *U* test. Data represent mean ± SEM. Sample number is indicated in the graph. Scale bar: 25μm.

that the subpopulation of primed Myh11-derived SMCs may be uniquely sensitive to radiation due to their increased plasticity, which would presumably be associated with a more open chromatin state that may increase their susceptibility to radiation-induced DNA damage independent of proliferation status. However, it will be extremely difficult to directly test this possibility, given that Sca1 is expressed by many cell types other than SMCs. As such, studies would require development of a sequential dual-recombinase lineage tracing mouse that allows selective lineage tracing of the subset of Myh11-expressing SMCs that subsequently activate Sca1.

An alternative possibility is that radiation may induce terminal differentiation of a proliferation-competent subset of medial SMCs exclusively in NC-derived vascular beds. This idea is supported by a previous study showing that radiation-induced coat graying, which is normally maintained by a NC-derived melanocyte stem cell population, was due to radiation-induced terminal differentiation of the stem cell population (27). To extrapolate from these studies, perhaps the SMC population primed to oligoclonally expand is terminally differentiated following radiation, impairing the ability of SMCs

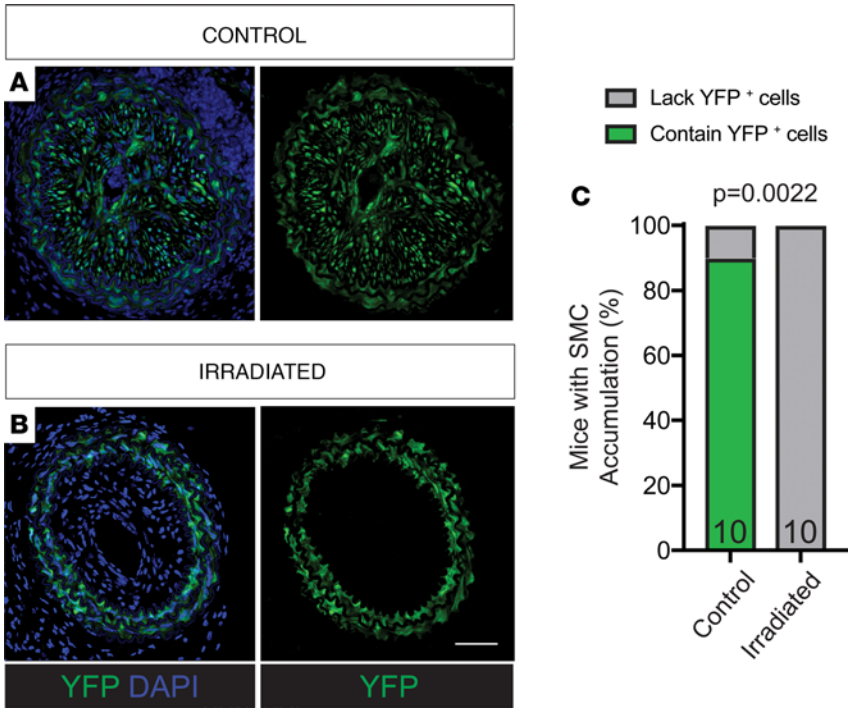


**Figure 5. The carotid artery neointima lacks YFP⁺ SMC investment following lethal irradiation and BMT.** (**A**) YFP⁺ SMC accumulate in the neointima that form after carotid ligation surgery. (**B**) Lethal irradiation ablated YFP⁺ cell accumulation in the carotid artery neointima. (**C**) Fisher's exact test quantifying the percentage of animals that demonstrate YFP⁺ cell accumulation in neointima with and without radiation. Sample number is indicated in the graph. Scale bar: 50 μm.

to populate BCA, carotid, and aortic arch lesions. However, the appropriate dual-lineage tracing mouse model systems required to test this hypothesis are also not currently available.

We believe that the results of these studies are of great interest to multiple fields of basic and clinical biology. However, the preceding points make it clear that many intrinsic and extrinsic mechanisms may be responsible for radiation selectively abrogating the ability of SMCs in the BCA, carotid artery, and aortic arch to invest into lesions. Thus, extensive further studies will be necessary to elucidate the underlying mechanisms for these effects, understand the possible implications of our results for clinical medicine, and interpret the findings of the more than 100,000 previous publications that have employed BMT as a primary experimental approach.

## Methods

### Animal handling and tissue processing

*Bone marrow transplant studies*. Studies were performed on male *Myh11*-CreER$^{T2}$, ROSA*26* STOP-flox eYFP$^{+/+}$ littermates backcrossed 9 times to C57BL/6 (8). Males were used, as the *Myh11*-CreER$^{T2}$ transgene is located on the Y chromosome. Mice used for atherosclerosis studies (Figure 1A) were crossed to an *Apoe*$^{-/-}$ background (SMC-YFP, *Apoe*$^{-/-}$), whereas carotid ligation studies were performed on both *Apoe*$^{-/-}$ and *Apoe*$^{+/+}$ mice (SMC-YFP). Cre-lox–mediated recombination of eYFP was induced in 6- to 8-week-old mice after intraperitoneal injections of 1 mg tamoxifen (T-5648, MilliporeSigma) per mouse per day for 10 days over 2 weeks. At 9 weeks of age, mice underwent lethal irradiation, receiving two 600-cGy doses, 3 hours apart, using a cesium-137 irradiator (Mark 1-68a; JL Shepard and Associates) and bone marrow was reconstituted 30–60 minutes later with >1 × 10$^6$ unfractionated bone marrow cells via tail vein injection, as previously described (28). 1,200 cGy was chosen as the dosage for lethal radiation in mice based on multiple previous reports. Bone marrow was harvested from the femurs and tibias from donors aged 4–7 weeks.

After BMT, mice were given antibiotics via drinking water (Sulfa water: 80 mg/ml sulfamethoxazole, 16 mg/ml trimethoprim, Teva Pharmaceuticals) for 6–7 weeks during bone marrow reconstitution before either being placed on WD to induce atherosclerosis development (Harlan Teklad, 21% milk fat, 0.15% cholesterol)

or undergoing carotid ligation (Figure 1, B and D). Alternatively, mice were harvested 1, 4, or 7 days after irradiation and BMT and given a single BrdU pulse at the time of radiation (10 mg/ml; MilliporeSigma, B5002; lot HMBF4669V), as were their corresponding nonirradiated, non-BMT control littermates (Figure 1C). On the day of harvest, and 12 hours after fasting (atherosclerosis only), mice were euthanized by $CO_2$ asphyxiation. Blood was drawn for testing prior to perfusion fixation via the left ventricle with 4% paraformaldehyde (PFA; EMS 15710) as previously described (8). To test hyperlipidemia, plasma cholesterol and triglyceride levels were analyzed by the University of Virginia Clinical Pathology Laboratory.

*Bone marrow donor mice*. Bone marrow for atherosclerosis studies and the studies on the acute effects of radiation was as follows: CD45.1 *Apoe*$^{-/-}$, tdTomato *Apoe*$^{-/-}$, or dsRed *Apoe*$^{-/-}$ derived from Tg(CAG-DsRed*MST)1Nagy/J (Jackson Laboratory, 005441). Bone marrow for mice in carotid ligation studies used marker tdTomato *Apoe*$^{+/+}$ derived from B6.129(Cg)-Gt(ROSA)26Sortm4(ACTB-tdTomato,-EGFP)Luo/J (Jackson Laboratory, 007676) or CD45.1 *Apoe*$^{-/-}$ derived from B6.SJL-Ptprca Pepcb/BoyJ (Jackson Laboratory, 002014), when appropriate. Bone marrow was harvested from donors between 4 and 7 weeks of age from the femur and tibia, and >1 × $10^6$ unfractionated bone marrow cells were injected via tail vein 30–60 minutes after radiation.

*Validating bone marrow reconstitution*. Blood samples were acquired by terminal cardiac puncture. Red blood cells and platelets were cleared using 1× RBC lysis buffer (BD PharmLyse, 555899) and 1× Hanks Balanced Salt Solution (Gibco, 14185). Prior to surface staining, Fc receptors were blocked with TruStain fcX anti-mouse CD16/32 antibody (Biolegend, 101320; 10 μg/ml). Dead cells were eliminated from the analysis using Live-Dead Fixable Yellow (Thermo Fisher, L34959; 0.55 μl/ml). Cells were stained with the following antibodies: CD45.1 (BD Pharmingen, clone A20; 2.5 μg/ml) and CD45.2 (eBiosciences, clone 104; 2.5 μg/ml). OneComp ebeads (eBiosciences, 01-1111-42; 50 μl/sample) were used for single-stain controls, and all experiments used fluorescent minus one controls for each marker. All samples were run on a Beckman Coulter CyAn ADP LX flow cytometer and analyzed using FlowJo v10.

*Atherosclerosis experimental design*. SMC-YFP, *Apoe*$^{-/-}$ mice for atherosclerosis studies were irradiated at 9 weeks of age with Sulfa water/bone marrow reconstitution for 6 weeks. Experiments were repeated 3 times, with mice ($n$ = 8; 1,200 cGy, $n$ = 7 control) receiving bone marrow from dsRed *Apoe*$^{-/-}$, tdTomato *Apoe*$^{-/-}$, or CD45.1 *Apoe*$^{-/-}$ donors. Mice were then placed on WD for 18 weeks. Littermate controls either received Sulfa water or normal drinking water for the same duration as experimental animals prior to WD feeding. There were no significant differences in control animals that received normal drinking water or Sulfa water. Studies used various bone marrow donors to rule out donor- or trace-dependent effects on atherosclerosis.

Various locations along the aortic tree that reliably develop lesions, including the BCA, aortic arch, aortic root, abdominal aorta, renal artery, and iliac artery just below the iliac bifurcation, were then excised, post-fixed in 4% PFA, and embedded in paraffin or put in a sucrose gradient and embedded in OCT (9). Given the recent finding that the ascending aorta is derived from both NC and secondary heart field, the aortic arch sections were taken between the BCA bifurcation and the left subclavian (Figure 1E) (29). All vessels were sectioned at 10 μm. The BCA samples were sectioned as previously described, starting past the aortic arch, which allows for lesion analysis at regular intervals. All other samples were sectioned entirely to include areas with lesion deposition (8).

*Carotid ligation and femoral injury experimental design*. Two groups of SMC-YFP (*Apoe*$^{+/+}$ or *Apoe*$^{-/-}$) mice underwent carotid ligation or femoral injury surgery, adapted from methods previously described (30–32). Briefly, mice that had undergone irradiation and BMT reconstitution or controls were put under anesthesia using the Kent Scientific SomnoSuite Isofluorane delivery system (3% v/wt, 250 ml/min). Once mice were anesthetized, 100 μl bupivacaine HCl (0.25% NDC 55150-167-10) was administered locally. Carotid ligations were performed by making a midline incision, and the left ($n$ = 5 control, $n$ = 5 irradiated) or right ($n$ = 5 control, $n$ = 5 irradiated) carotid artery was exposed. A 7-0 suture was placed immediately proximal to the internal/external carotid bifurcation. To induce femoral injury, a straight spring wire was inserted into the left femoral artery. The wire was advanced and retracted in a sawing motion 10 times to denude the endothelium and produce neointimal hyperplasia. The collateral artery immediately proximal to the deep femoral artery was also ligated to induce neointima formation of lesser severity. The contralateral carotid or femoral artery served as an uninjured control. Mice were euthanized 21 days after ligation, and the arteries were excised, post-fixed in 4% PFA, and embedded in paraffin. Vessels were sectioned at 10 μm from ligation through the first 1.5–2.5 mm for analysis.

## Immunohistochemical analysis

*Staining protocols*. Paraffin-embedded samples were deparaffinized prior to antigen retrieval (Vector Laboratories, H-3300) and staining. Immunofluorescence staining of vessel sections was performed as previously described (8) to evaluate protein expression in single cells (based on DAPI$^+$ nuclei) with primary antibodies specific for GFP (Abcam, ab6673; 1:250), cleaved caspase-3 (Cell Signaling, 9661S; 1:75), MKi67 (Abcam, ab15580; 1:250), or IgG as an internal negative control. TUNEL staining was performed using the CF 640R TUNEL Assay Apoptosis Detection Kit (Biotium, 30074; lot 180417). Cells were counter stained with DAPI (Thermo Fisher Scientific, D3571). Secondary antibodies for immunofluorescence included the following: donkey anti-goat AF-488 (Invitrogen, A11055; 1:250), donkey anti-rabbit AF-555 (Invitrogen, A31572; 1:250), donkey anti-goat AF-647 (Invitrogen, A21447; 1:250).

Vessel and lesion morphometry analysis was performed using Modified Russel-Movat (Movat) staining at 3 locations along the BCA to assess vessel and lesion areas. To assess intraplaque hemorrhage at 3 locations along the BCA, red blood cells were visualized with Ter119 primary antibody (Santa Cruz Biotechnology Inc., 1:200), and biotinylated secondary antibody (Vector, BA-4001, 1:200) and visualized with 3′,3-diaminobenzidine (Acros Organic) as previously described (10). To assess collagen at two locations along the BCA, Picrosirius red was used for visualization of mature collagen fibrils by birefringence under polarized light (10). Necrotic core analyses were assessed based on the bright-field images from Picrosirius red staining and were performed by two investigators independently.

*Image acquisition and analysis*. Immunofluorescence imaging of vessel sections was performed using a Zeiss LSM700 confocal microscope. Figure images were acquired at 2,048 × 2,048 resolution using a ×20 magnification at 0.5 zoom. A series of 1 μm *Z*-stack images were acquired for single-cell detection within the lesion or media. Figure images are orthogonal projections of *Z*-stacks, with background fluorescence decreased (background fluorescence was considered if unassociated with DAPI$^+$ nucleus) in both experimental and control animals and were performed using Zen Light Edition Software (Zeiss). Figure images were pseudo-colored and YFP signal was brightened with gamma expansion for visualization in print, and scale bars were added in Adobe Photoshop.

Movat- and Ter119-stained images were acquired with a Zeiss Axioskope2 fitted with an AxioCamMR3 camera, using AxioVision40 V4.6.3.0 software (Carl Zeiss Imaging Solution). Settings were standardized for each staining protocol and used for the entirety of image acquisition. Picrosirius red images were taken using an Olympus BX51 under a polarized lens. Vessel morphometry and areas of positive immunohistochemical or Picrosirius red staining within defined areas of interest were quantified using ImagePro Plus 7.0 software (Media Cybernetics Inc.).

## Genotyping primers

The following primers were used: *eYFP*, GGAGCGGGAGAAATGGATATG, AAGTTCATCTGCACCACCG, TCCTTGAAGAAGATGGTGCG, and CGTGATCTGCAACTCCAGTC; *Myh11-Cre*, TGACCCCATCTCTTCACTCC, AACTCCACGACCACCTCATC, and AGTCCCTCACATCCTCAGGTT; *Apoe*, GCCTAGCCGAGGGAGAGCCG, TGTGACTTGGGAGCTCTGCAGC, and GCCGCCCCGACTGCATCT; *tdTomato*, AAGGGAGCTGCAGTGGAGTA, CGGGCCATTTACCGTAAGTTAT, and CCGAAAATCTGTGGGAAGTC; *CD45.1*, CTCACAGGCACATGAACGAT and CGCTTCAAGCATGTCTTCTG; and *dsRed*, CCCATGGTCTTCTTCTGCAT, AAGGTGTACGTGAAGCACCC, CTAGGCCACAGAATTGAAAGATCT, and GTAGGTGGAAATTCTAGCATCATCC.

## Statistics

Statistics were calculated using GraphPad Prism software v7. SMC investment into lesions and intraplaque hemorrhage were analyzed by 2-sided Baptista-Pike Fisher exact test, with odds ratio and 95% confidence interval. Vessel morphometry, necrotic core, and Picrosirius red images were analyzed using 2-way ANOVA with multiple comparisons and Bonferroni correction. Data are presented as mean ± SEM. All *P* values reflect significant differences between control and experimental groups, and numbers of animal are shown within figures. A *P* value of less than 0.05 was considered significant.

## Study approval

Animal protocols were reviewed and approved by the Institutional Animal Care and Use Committee at the University of Virginia.

## Author contributions

AACN and RAB performed the bulk of the experiments, data collection and analysis, and wrote the manuscript. DLH performed surgeries and contributed editorially to the manuscript. SDG performed surgeries and contributed to data collection. LSS initiated BMT studies. OAC performed surgeries and provided guidance throughout the project. All authors conceived of and intellectually contributed to the experimental design. GKO supervised the entire project and had a major role in experimental design, data interpretation, and writing the manuscript.

## Acknowledgments

The authors thank D. Gomez and B.G. Durgin for their input, and acknowledge A. Saenz and C.M. Kasden for help with tissue harvest, A. Washington for assistance with histology, T.C.S. Keller IV for assistance with data collection, A. Young for performing surgeries, and the University of Virginia Center for Comparative Medicine for use of equipment and support. This work was supported by NIH grants R01 HL057353, HL121008, HL136314, and HL132904 (to GKO); NIH grant T32 HL007284 (to AACN, RAB, SDG, and LSS); American Heart Association grant 17IRG33370017 (to OAC); and NIH grant F30 HL136188 (to RAB).

Address correspondence to: Gary K. Owens, University of Virginia School of Medicine, 415 Lane Road, PO Box 801394, Room 1322 Medical Research Building 5, Charlottesville, Virginia 22908, USA. Phone: 434.924.2652; Email: gko@virginia.edu.

1. Lorenz E, Congdon C, Uphoff D. Modification of acute irradiation injury in mice and guinea-pigs by bone marrow injections. *Radiology*. 1952;58(6):863–877.
2. Gratwohl A, et al. One million haemopoietic stem-cell transplants: a retrospective observational study. *Lancet Haematol*. 2015;2(3):e91–100.
3. Mertens AC, et al. Cause-specific late mortality among 5-year survivors of childhood cancer: the Childhood Cancer Survivor Study. *J Natl Cancer Inst*. 2008;100(19):1368–1379.
4. Darby SC, et al. Risk of ischemic heart disease in women after radiotherapy for breast cancer. *N Engl J Med*. 2013;368(11):987–998.
5. Stewart FA, et al. Ionizing radiation accelerates the development of atherosclerotic lesions in ApoE-/- mice and predisposes to an inflammatory plaque phenotype prone to hemorrhage. *Am J Pathol*. 2006;168(2):649–658.
6. Schiller NK, Kubo N, Boisvert WA, Curtiss LK. Effect of gamma-irradiation and bone marrow transplantation on atherosclerosis in LDL receptor-deficient mice. *Arterioscler Thromb Vasc Biol*. 2001;21(10):1674–1680.
7. Gabriels K, et al. Irradiation of existing atherosclerotic lesions increased inflammation by favoring pro-inflammatory macrophages. *Radiother Oncol*. 2014;110(3):455–460.
8. Gomez D, Shankman LS, Nguyen AT, Owens GK. Detection of histone modifications at specific gene loci in single cells in histological sections. *Nat Methods*. 2013;10(2):171–177.
9. Shankman LS, et al. KLF4-dependent phenotypic modulation of smooth muscle cells has a key role in atherosclerotic plaque pathogenesis. *Nat Med*. 2015;21(6):628–637.
10. Cherepanova OA, et al. Activation of the pluripotency factor OCT4 in smooth muscle cells is atheroprotective. *Nat Med*. 2016;22(6):657–665.
11. Murry CE, Gipaya CT, Bartosek T, Benditt EP, Schwartz SM. Monoclonality of smooth muscle cells in human atherosclerosis. *Am J Pathol*. 1997;151(3):697–705.
12. Chappell J, et al. Extensive proliferation of a subset of differentiated, yet plastic, medial vascular smooth muscle cells contributes to neointimal formation in mouse injury and atherosclerosis models. *Circ Res*. 2016;119(12):1313–1323.
13. Jacobsen K, et al. Diverse cellular architecture of atherosclerotic plaque derives from clonal expansion of a few medial SMCs. *JCI Insight*. 2017;2(19):e95890.
14. Durgin BG, et al. Smooth muscle cell-specific deletion of Col15a1 unexpectedly leads to impaired development of advanced atherosclerotic lesions. *Am J Physiol Heart Circ Physiol*. 2017;312(5):H943–H958.
15. Majesky MW. Developmental basis of vascular smooth muscle diversity. *Arterioscler Thromb Vasc Biol*. 2007;27(6):1248–1258.
16. Gadson PF, et al. Differential response of mesoderm- and neural crest-derived smooth muscle to TGF-beta1: regulation of c-myb and alpha1 (I) procollagen genes. *Exp Cell Res*. 1997;230(2):169–180.
17. Jaffe M, et al. Transforming growth factor-β signaling in myogenic cells regulates vascular morphogenesis, differentiation, and matrix synthesis. *Arterioscler Thromb Vasc Biol*. 2012;32(1):e1–11.
18. Topouzis S, Majesky MW. Smooth muscle lineage diversity in the chick embryo. Two types of aortic smooth muscle cell differ in growth and receptor-mediated transcriptional responses to transforming growth factor-beta. *Dev Biol*. 1996;178(2):430–445.
19. Lee MO, et al. Effect of ionizing radiation induced damage of endothelial progenitor cells in vascular regeneration. *Arterioscler Thromb Vasc Biol*. 2012;32(2):343–352.
20. Kirby ML, Waldo KL. Neural crest and cardiovascular patterning. *Circ Res*. 1995;77(2):211–215.
21. Bergonie J, Tribondeau L. Interpretation of some results of radiotherapy and an attempt at determining a logical technique of treatment. *Radiat Res*. 1959;11:587–588.
22. Reidy MA. Proliferation of smooth muscle cells at sites distant from vascular injury. *Arteriosclerosis*. 1990;10(2):298–305.
23. Olson NE, Chao S, Lindner V, Reidy MA. Intimal smooth muscle cell proliferation after balloon catheter injury. The role of

basic fibroblast growth factor. *Am J Pathol*. 1992;140(5):1017–1023.
24. Jiang X, Rowitch DH, Soriano P, McMahon AP, Sucov HM. Fate of the mammalian cardiac neural crest. *Development*. 2000;127(8):1607–1616.
25. Sheikh AQ, Misra A, Rosas IO, Adams RH, Greif DM. Smooth muscle cell progenitors are primed to muscularize in pulmonary hypertension. *Sci Transl Med*. 2015;7(308):308ra159.
26. Majesky MW, et al. Differentiated smooth muscle cells generate a subpopulation of resident vascular progenitor cells in the adventitia regulated by Klf4. *Circ Res*. 2017;120(2):296–311.
27. Inomata K, et al. Genotoxic stress abrogates renewal of melanocyte stem cells by triggering their differentiation. *Cell*. 2009;137(6):1088–1099.
28. Iwata H, et al. Bone marrow-derived cells contribute to vascular inflammation but do not differentiate into smooth muscle cell lineages. *Circulation*. 2010;122(20):2048–2057.
29. Sawada H, Rateri DL, Moorleghen JJ, Majesky MW, Daugherty A. Smooth muscle cells derived from second heart field and cardiac neural crest reside in spatially distinct domains in the media of the ascending aorta-Brief report. *Arterioscler Thromb Vasc Biol*. 2017;37(9):1722–1726.
30. Takayama T, et al. A murine model of arterial restenosis: Technical aspects of femoral wire injury. *J Vis Exp*. 2015;(97):52561.
31. Herring BP, Hoggatt AM, Burlak C, Offermanns S. Previously differentiated medial vascular smooth muscle cells contribute to neointima formation following vascular injury. *Vasc Cell*. 2014;6(1):21.
32. Le V, Johnson CG, Lee JD, Baker AB. Murine model of femoral artery wire injury with implantation of a perivascular drug delivery patch. *J Vis Exp*. 2015;(96):52403.